Available online at www.sciencedirect.com
ScienceDirect
Journal of Sound and Vibration 320 (2009) 545–558
JOURNAL OF SOUND AND VIBRATION
www.elsevier.com/locate/jsvi

Design variable tolerance effects on the natural frequency variance of constrained multi-body systems in dynamic equilibrium

Bum Seok Kim[a,1], Seung Man Eom[b,2], Hong Hee Yoo[a,*]

[a]School of Mechanical Engineering, Hanyang University, 17 Haengdang-Dong Sungdong-Gu, Seoul 133-791, South Korea
[b]Aircraft Development Team, Korea Institute of Aerospace Technology, 461-1 Junmin-Dong Yusung-Gu, Daejeon 305-811, South Korea

Received 13 March 2008; received in revised form 31 July 2008; accepted 15 August 2008
Handling Editor: J. Lam
Available online 8 October 2008

Abstract

The design variable tolerance effects on the natural frequency variance of constrained multi-body systems in dynamic equilibrium are investigated in this study. Monte-Carlo simulation is often employed for such investigations, but it is known to have serious drawbacks. Excessive amount of computation time needs to be consumed since a large number of evaluations are usually required for the method. Furthermore, the solution accuracy cannot be always guaranteed in spite of the excessive amount of computation time. In order to overcome such drawbacks, a method employing eigenvalue sensitivity information is proposed to obtain the variance of natural frequency in this study. In order to verify the accuracy and the efficiency of the method, some numerical examples of multi-body systems in dynamic equilibrium are solved and the results are compared to those obtained by an analytical method and Monte-Carlo simulation.

1. Introduction

A dynamic equilibrium state can be often found in a mechanical system in which a part of the system undergoes constant rotational motion. Such systems having rotating parts include governor mechanisms, turbomachines and amusement park rides. In a state of dynamic equilibrium of a mechanical system, some of the generalized coordinates remain constant while the others may vary with time. In order to find the constant generalized coordinates of a constrained multi-body system in dynamic equilibrium, a general multi-body formulation was proposed (see Ref. [1]). A velocity transformation (see Ref. [2]) along with relative coordinates (see Refs. [3,4]) was employed for the formulation, and nonlinear algebraic equations were obtained and numerically solved by using an iterative method.

*Corresponding author. Tel.: +82 2 2220 0446; fax: +82 2 2293 5070.
E-mail addresses: apenny@hanmail.net (B.S. Kim), yoltne@empal.com (S.M. Eom), hhyoo@hanyang.ac.kr (H.H. Yoo).
[1]Tel.: +82 2 2299 8169; fax: +82 2 2293 5070.
[2]Tel.: +82 42 868 6077; fax: +82 42 868 6128.

0022-460X/$ - see front matter © 2008 Elsevier Ltd. All rights reserved.
doi:10.1016/j.jsv.2008.08.015

In 1986, a pioneering method for determining the modal characteristics of a general multi-body system was introduced by Sohoni and Whitesell [5]. With the purpose to find the modal characteristics of a constrained multi-body system in static equilibrium, they derived and solved an eigenvalue problem for which the mass, damping and stiffness matrices were obtained from a general multi-body formulation. However, the modal characteristics of a multi-body system in dynamic equilibrium could not be obtained with the method. More recently, Choi et al. [6] proposed a method to find the modal characteristics of a multi-body system in dynamic equilibrium. The equations of motion employing relative coordinates were first derived and then linearized around a dynamic equilibrium position so that an eigenvalue problem could be derived and solved. Since the static equilibrium is only a special case of the dynamic equilibrium, this method is more general than the Sohoni and Whitesell method.

With the intent to design a multi-body system which operates around a dynamic equilibrium position, the dynamic equilibrium position and the corresponding modal characteristics need to be obtained accurately and efficiently. Moreover, the effects of design variable tolerances on the variance of modal characteristics should be also obtained accurately and efficiently for the design of the multi-body system. Such information is crucial for robust system design, since excessive variance of modal characteristics of a mechanical system should be avoided during the life time operation.

Over the last years, the effects of various design variable tolerances on the motion errors of mechanical linkage systems have been investigated by many researchers. In 1964, Hartenberg and Denavit [7] first addressed the issue of mechanical errors in linkages due to tolerances. They estimated the mechanical errors based on the maximum allowable tolerances of the link lengths in four-bar linkages. Their method employed a deterministic approach and offered a 'worst case' result due to a tolerance. Garret and Hall [8] developed a statistical approach to determine mechanical errors due to link length tolerances and joint clearances. They represented the error as a mobility band and carried out Monte-Carlo simulations for a four-bar linkage system. More recently, Lee [9] proposed an effective link model for which an analytic formulation employing the first-order Taylor series expansion was employed. Lee and Gilmore [10] later considered the uncertainties due to the tolerances of pin location, link length, and the radial clearance as variations of the effective link model. More recently, several research results (see Refs. [11–15]) related to the joint clearance were published.

Most of the above studies limited themselves to the tolerance effects on the motion errors of mechanical systems, rarely studying the tolerance effects on the variances of other characteristics. Furthermore, most of them were limited to linkage systems. So, specific formulations for certain linkage systems were used for the studies. A general multi-body formulation has rarely been employed to analyze the tolerance effects on the performance or characteristic variances of mechanical systems. The purpose of the present study is to present an efficient and systematic method to investigate the tolerance effects on the modal characteristic variances of general multi-body systems in dynamic equilibrium. In particular, the modal characteristic variances of general multi-body systems undergoing rotational motion are investigated in this study. The accuracy and the efficiency of the proposed method are compared to those of an analytical method and Monte-Carlo simulation through some numerical examples.

2. Equations of motion for multi-body systems in dynamic equilibrium

The augmented Lagrange equations of motion for a constrained multi-body system (see Refs. [16–19]) are generally written in terms of Cartesian coordinates as follows:

$$\mathbf{M}\ddot{\mathbf{x}} + \mathbf{\Phi}_{\mathbf{x}}^{\mathrm{T}}\boldsymbol{\lambda} = \mathbf{Q} \tag{1}$$

where $\mathbf{M}$ denotes a mass matrix, $\mathbf{Q}$ denotes a generalized force vector, $\boldsymbol{\lambda}$ denotes the Lagrange multiplier vector, and $\mathbf{\Phi}_{\mathbf{x}}$ is called the Jacobean matrix, which is the derivative of the constraint equations $\mathbf{\Phi}$ with respect to a set of Cartesian coordinates $\mathbf{x}$.

When a constrained multi-body system is in dynamic equilibrium, its relative configuration becomes fixed. Therefore, it is much more efficient to employ relative coordinates to find the dynamic equilibrium of a constrained multi-body system. In order to derive the equations of motion in terms of a set of relative coordinates (which is hereafter denoted as $\mathbf{q}$), a velocity transformation method is employed. The Cartesian

velocity vector $\dot{\mathbf{x}}$ is related to the relative velocity vector $\dot{\mathbf{q}}$ as follows:

$$\dot{\mathbf{x}} = \mathbf{B}\dot{\mathbf{q}} \tag{2}$$

where $\mathbf{B}$ denotes the velocity transformation matrix between the two velocity vectors.

In order to derive the equations of motion for a constrained multi-body system undergoing constant rotational motion, the system coordinates are partitioned into $\mathbf{q_D}$ (coordinates which are involved with the constant rotational motion) and $\mathbf{q_R}$ (the rest of the relative coordinates). Thus,

$$\mathbf{q} = \begin{bmatrix} \mathbf{q}_\mathbf{D}^\mathrm{T} & \mathbf{q}_\mathbf{R}^\mathrm{T} \end{bmatrix}^\mathrm{T} \tag{3}$$

Now, the Cartesian velocity vector $\dot{\mathbf{x}}$ is related to $\dot{\mathbf{q}}_\mathbf{D}$ and $\dot{\mathbf{q}}_\mathbf{R}$ as follows:

$$\dot{\mathbf{x}} = \mathbf{B_D}\dot{\mathbf{q}}_\mathbf{D} + \mathbf{B_R}\dot{\mathbf{q}}_\mathbf{R} \tag{4}$$

where the velocity transformation matrices $\mathbf{B_D}$ and $\mathbf{B_R}$ are sub-matrices associated with the velocity vectors $\dot{\mathbf{q}}_\mathbf{D}$ and $\dot{\mathbf{q}}_\mathbf{R}$. Therefore, $\mathbf{B}$ is composed of $\mathbf{B_D}$ and $\mathbf{B_R}$ as follows:

$$\mathbf{B} = \begin{bmatrix} \mathbf{B_D} & \mathbf{B_R} \end{bmatrix} \tag{5}$$

By taking the time derivative of Eq. (4), the following equation can be obtained:

$$\ddot{\mathbf{x}} = \mathbf{B_D}\ddot{\mathbf{q}}_\mathbf{D} + \mathbf{B_R}\ddot{\mathbf{q}}_\mathbf{R} + \dot{\mathbf{B}}_\mathbf{D}\dot{\mathbf{q}}_\mathbf{D} + \dot{\mathbf{B}}_\mathbf{R}\dot{\mathbf{q}}_\mathbf{R} \tag{6}$$

Substituting Eq. (6) into Eq. (1) and pre-multiplying the result by $\mathbf{B}_\mathbf{R}^\mathrm{T}$, the equations of motion can be obtained (for an open-loop system) as

$$\mathbf{M}^*\ddot{\mathbf{q}}_\mathbf{R} = \mathbf{Q}^* \tag{7}$$

where

$$\mathbf{M}^* = \mathbf{B}_\mathbf{R}^\mathrm{T}\mathbf{M}\mathbf{B_R} \tag{8}$$

$$\mathbf{Q}^* = \mathbf{B}_\mathbf{R}^\mathrm{T}(\mathbf{Q} - \mathbf{M}\mathbf{B_D}\ddot{\mathbf{q}}_\mathbf{D} - \mathbf{M}\,\dot{\mathbf{B}}_\mathbf{D}\,\dot{\mathbf{q}}_\mathbf{D} - \mathbf{M}\,\dot{\mathbf{B}}_\mathbf{R}\,\dot{\mathbf{q}}_\mathbf{R}) \tag{9}$$

At the dynamic equilibrium state, $\dot{\mathbf{q}}_\mathbf{R}$, $\ddot{\mathbf{q}}_\mathbf{R}$, and $\ddot{\mathbf{q}}_\mathbf{D}$ become zero, while $\dot{\mathbf{q}}_\mathbf{D}$ is constant. Therefore, the following equilibrium equation can be obtained from Eq. (7):

$$\mathbf{B}_\mathbf{R}^\mathrm{T}(\mathbf{Q} - \mathbf{M}\,\dot{\mathbf{B}}_\mathbf{D}\,\dot{\mathbf{q}}_\mathbf{D}) = \mathbf{0} \tag{10}$$

Eq. (10) constitutes algebraic equations from which the values of the coordinates $\mathbf{q_R}$ should be found. A numerical method using an iterative scheme, such as the Newton–Raphson method, is usually employed to find the equilibrium state values since Eq. (10) is nonlinear in terms of $\mathbf{q_R}$.

For the modal analysis of the system, the following homogeneous linear equation can be obtained by linearizing Eq. (7):

$$\hat{\mathbf{M}}\,\ddot{\mathbf{q}}_\mathbf{R} + \hat{\mathbf{C}}\,\dot{\mathbf{q}}_\mathbf{R} + \hat{\mathbf{K}}\,\mathbf{q}_\mathbf{R} = 0 \tag{11}$$

where $\hat{\mathbf{M}}$, $\hat{\mathbf{C}}$ and $\hat{\mathbf{K}}$, which denote mass, damping and stiffness matrices, respectively, can be obtained as follows:

$$\hat{\mathbf{M}} = \mathbf{B}_\mathbf{R}^\mathrm{T}\mathbf{M}\mathbf{B_R}|_{\mathbf{q}_\mathbf{R}^*} \tag{12}$$

$$\hat{\mathbf{C}} = -\left.\frac{\partial \mathbf{Q}^*}{\partial \dot{\mathbf{q}}_\mathbf{R}}\right|_{\mathbf{q}_\mathbf{R}^*} \tag{13}$$

$$\hat{\mathbf{K}} = -\left.\frac{\partial \mathbf{Q}^*}{\partial \mathbf{q}_\mathbf{R}}\right|_{\mathbf{q}_\mathbf{R}^*} \tag{14}$$

where $\mathbf{q}_\mathbf{R}^*$ denotes the value of $\mathbf{q_R}$ at the dynamic equilibrium. Eq. (12) can be obtained directly from Eq. (8). Eqs. (13) and (14) can be obtained by linearizing Eq. (9) with respect to $\dot{\mathbf{q}}_\mathbf{R}$ and $\mathbf{q_R}$. Analytical derivation

procedures of the damping and the stiffness matrices are much complicated. So, the finite difference method is employed to obtain the damping and the stiffness matrices in the present work.

If the system is a closed-loop system, the equations of motion of a constrained multi-body system can be derived (see Ref. [20]) as follows:

$$\mathbf{M}^*\ddot{\mathbf{q}}_\mathbf{R} + \mathbf{\Phi}^{c\mathrm{T}}_{\mathbf{q}_\mathbf{R}}\boldsymbol{\lambda}^c = \mathbf{Q}^* \tag{15}$$

where $\mathbf{\Phi}^c$ denotes the constraint equations which are involved with the cut joints of the system, $\boldsymbol{\lambda}^c$ denotes the corresponding Lagrange multiplier vector, and $\mathbf{\Phi}^c_{\mathbf{q}_\mathbf{R}}$ denotes the derivative of $\mathbf{\Phi}^c$ with respect to $\mathbf{q}_\mathbf{R}$.

At the dynamic equilibrium state, the following equation can be obtained:

$$\mathbf{B}^{\mathrm{T}}_\mathbf{R}(\mathbf{Q} - \mathbf{M}\dot{\mathbf{B}}_\mathbf{D}\dot{\mathbf{q}}_\mathbf{D}) - \mathbf{\Phi}^{c\mathrm{T}}_{\mathbf{q}_\mathbf{R}}\boldsymbol{\lambda}^c = \mathbf{0} \tag{16}$$

In order to obtain the dynamic equilibrium position, the above equation along with $\mathbf{\Phi}^c = 0$ should be solved simultaneously. In a similar way to an open-loop system discussed previously, an iterative method should be employed to find the equilibrium state. In this case, $\boldsymbol{\lambda}^c$ as well as $\mathbf{q}_\mathbf{R}$ is obtained.

For a closed-loop system, the $\mathbf{q}_\mathbf{R}$'s are not all independent. So let us say that $\mathbf{u}$ denotes the dependent coordinates of $\mathbf{q}_\mathbf{R}$ and $\mathbf{v}$ denotes the independent coordinates of $\mathbf{q}_\mathbf{R}$. The number of the independent coordinates $\mathbf{v}$ depends on the type of the joints of the closed loops. As long as the number of $\mathbf{v}$ is correct one can freely choose the independent coordinates from $\mathbf{q}_\mathbf{R}$. Then, the following equation can be written:

$$\mathbf{\Phi}^{c\mathrm{T}}_\mathbf{u}\dot{\mathbf{u}} + \mathbf{\Phi}^{c\mathrm{T}}_\mathbf{v}\dot{\mathbf{v}} = \mathbf{0} \tag{17}$$

Now, the following equation can be obtained with the above equation:

$$\dot{\mathbf{q}}_\mathbf{R} = \mathbf{R}\dot{\mathbf{v}} \tag{18}$$

where

$$\mathbf{R} = \begin{bmatrix} -(\mathbf{\Phi}^{c\mathrm{T}}_\mathbf{u})^{-1}\mathbf{\Phi}^{c\mathrm{T}}_\mathbf{v} \\ \mathbf{I} \end{bmatrix} \tag{19}$$

Substituting Eq. (18) into Eq. (15) and pre-multiplying the result by $\mathbf{R}^{\mathrm{T}}$, the equations of motion can be rewritten as follows:

$$\mathbf{R}^{\mathrm{T}}\mathbf{M}^*\mathbf{R}\ddot{\mathbf{v}} + \mathbf{R}^{\mathrm{T}}\mathbf{M}^*\dot{\mathbf{R}}\,\dot{\mathbf{v}} - \mathbf{R}^{\mathrm{T}}\mathbf{Q}^* = 0 \tag{20}$$

From the above equation, the following homogeneous linear equation can be obtained for the modal analysis of the system:

$$\hat{\mathbf{M}}\,\ddot{\mathbf{v}} + \hat{\mathbf{C}}\,\dot{\mathbf{v}} + \hat{\mathbf{K}}\,\mathbf{v} = 0 \tag{21}$$

where $\hat{\mathbf{M}}$, $\hat{\mathbf{C}}$ and $\hat{\mathbf{K}}$ can be obtained as follows:

$$\hat{\mathbf{M}} = \mathbf{R}^{\mathrm{T}}\mathbf{B}^{\mathrm{T}}_\mathbf{R}\mathbf{M}\mathbf{B}_\mathbf{R}\mathbf{R}|_{\mathbf{v}^*} \tag{22}$$

$$\hat{\mathbf{C}} = \frac{\partial}{\partial\dot{\mathbf{q}}_\mathbf{R}}\mathbf{R}^{\mathrm{T}}[\mathbf{Q}^* - \mathbf{M}^*\dot{\mathbf{R}}\,\dot{\mathbf{v}}]|_{\mathbf{v}^*} \tag{23}$$

$$\hat{\mathbf{K}} = \frac{\partial}{\partial\mathbf{q}_\mathbf{R}}\mathbf{R}^{\mathrm{T}}[\mathbf{Q}^* - \mathbf{M}^*\dot{\mathbf{R}}\,\dot{\mathbf{v}}]|_{\mathbf{v}^*} \tag{24}$$

where $\mathbf{v}^*$ denotes the value of $\mathbf{v}$ at the dynamic equilibrium. Again, Eq. (22) can be employed directly to calculate the mass matrix. However, the finite difference method is employed to calculate the damping and the stiffness matrices numerically.

3. Sensitivity and tolerance analysis

The eigenvalue problem of a damped system can be stated (see Ref. [21]) as follows:

$$(\lambda_j^2\hat{\mathbf{M}} + \lambda_j\hat{\mathbf{C}} + \hat{\mathbf{K}})\phi_j = 0 \tag{25}$$

where ϕ_j denotes the normalized mode vector and λ_j denotes the corresponding eigenvalue. Differentiating Eq. (25) with respect to a design variable b, one can obtain

$$\left(\lambda_j^2\hat{\mathbf{M}} + \lambda_j\hat{\mathbf{C}} + \hat{\mathbf{K}}\right)\frac{\partial\phi_j}{\partial b} + \frac{\partial\lambda_j}{\partial b}(2\lambda_j\hat{\mathbf{M}} + \hat{\mathbf{C}})\phi_j + \left(\lambda_j^2\frac{\partial\hat{\mathbf{M}}}{\partial b} + \lambda_j\frac{\partial\hat{\mathbf{C}}}{\partial b} + \frac{\partial\hat{\mathbf{K}}}{\partial b}\right)\phi_j = 0 \tag{26}$$

Pre-multiplying Eq. (26) by ϕ_j^{T}, and employing Eq. (25) and the normalized condition $\phi_j^{\mathrm{T}}(2\lambda_j\hat{\mathbf{M}} + \hat{\mathbf{C}})\phi_j = 1$, the sensitivity of the eigenvalue λ_j for the design variable b can be obtained as follows:

$$\frac{\partial\lambda_j}{\partial b} = -\phi_j^{\mathrm{T}}\left(\lambda_j^2\frac{\partial\hat{\mathbf{M}}}{\partial b} + \lambda_j\frac{\partial\hat{\mathbf{C}}}{\partial b} + \frac{\partial\hat{\mathbf{K}}}{\partial b}\right)\phi_j \tag{27}$$

Unless the damping matrix has a special form (such as a proportional damping matrix) complex eigenvalues are obtained from the eigenvalue problem of Eq. (25). Since the imaginary parts of complex eigenvalues represent the damped natural frequencies, the sensitivity of the damped natural frequencies for the design variable b is the imaginary part of $\partial\lambda_j/\partial b$. If $\hat{\mathbf{M}}$, $\hat{\mathbf{C}}$ and $\hat{\mathbf{K}}$ matrices are given in analytical forms, the sensitivity information can be obtained analytically. However, for general multi-body systems, $\hat{\mathbf{M}}$, $\hat{\mathbf{C}}$ and $\hat{\mathbf{K}}$ matrices are not given in analytical forms. So, in general, the sensitivities of the matrices should be found numerically.

If the samples of the design variable b have a normal distribution with 99.73% confidence interval, the variance of a damped natural frequency can be obtained (see Refs. [22,23]) by the following equation:

$$\sigma_j = \frac{1}{3}\left(\frac{\partial\lambda_j}{\partial b}\right)T \tag{28}$$

where T denotes the tolerance of the design variable b, and the standard deviation of the jth damped natural frequency is the imaginary part of σ_j.

The first-order variance information is only employed to obtain the mean value in this study. In order to increase the accuracy of the mean value, the second-order variance information should be employed. However, the second-order variance information can be only obtained with the third and the fourth moments of b, which are not practically available. In most practical problems, the first-order variance information is sufficient to obtain accurate mean values. With this information the imaginary part of λ_j becomes the mean value of the jth damped natural frequency regardless of the tolerance of the design variable b.

4. Numerical results

In this section, some numerical results obtained with some multi-body system examples such as a double pendulum and a governor mechanism are exhibited to demonstrate the efficiency and the accuracy of the methodology proposed in this study.

Fig. 1 shows a double pendulum system undergoing a rotational motion. Each pendulum arm is a uniform homogeneous bar having a mass of 3 kg and length of 1 m. The two pendulum arms are connected by a pin joint, and the first pendulum arm is connected to a vertical shaft which undergoes a constant rotational motion. The angle between the vertical shaft and the first pendulum arm is denoted as θ_1, and that between the vertical shaft and the second pendulum arm is denoted as θ_2.

Fig. 2 shows the variations of the angles θ_1 and θ_2 at the dynamic equilibrium state versus the driving angular speed. The pendulum arms remain vertical until the angular speed reaches a certain value (2.679 rad/s). The virtual moment created by the gravitational force is larger than that created by the centrifugal inertial force until the angular speed reaches the value (2.679 rad/s). As the angular speed increases after exceeding the value, the equilibrium angles θ_1 and θ_2 increase and converge to a value of $\pi/2$ radian.

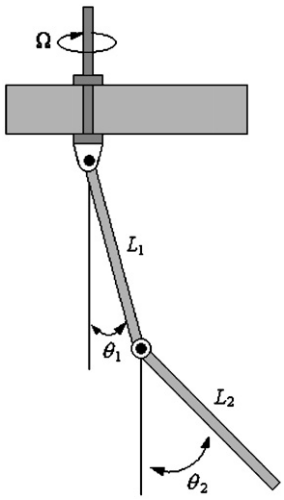

Fig. 1. Configuration of the rotating double pendulum.

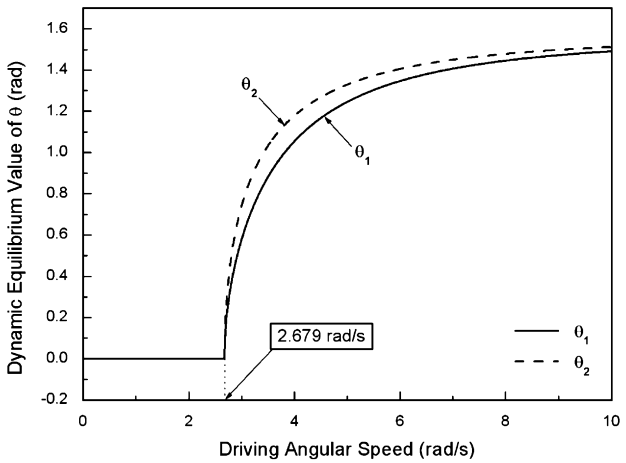

Fig. 2. Variations of the dynamic equilibrium angles θ_1 and θ_2 versus the driving angular speed.

Of course, θ_2 should be always larger than θ_1 since the second pendulum arm undertakes a larger moment created by the centrifugal inertia force.

Fig. 3 shows the variations of the first and the second natural frequencies versus the driving angular speed. As shown in the figure, the first and the second natural frequencies decrease until the angular speed reaches 2.679 rad/s. The first natural frequency especially becomes null at the angular speed. After reaching the minimum values at the angular speed, the two natural frequencies increase monotonically as the angular speed increases. Since this example is very simple, its equations of motion can be derived directly and the sensitivity information can be obtained analytically from the equations.

Fig. 4 shows the mean values of the natural frequencies versus the driving angular speed. The length of the two pendulum arms is assumed to have a normal distribution with 99.73% confidence. Three cases of pendulum arm length tolerances (3.0%, 6.0%, and 12.0%) are considered for the Monte-Carlo simulation. The mean values obtained by the proposed method are plotted too. As shown, the results obtained by the proposed methods are in good agreement with those obtained by the Monte-Carlo simulation, indicating trivial differences among the results obtained with the three different tolerances.

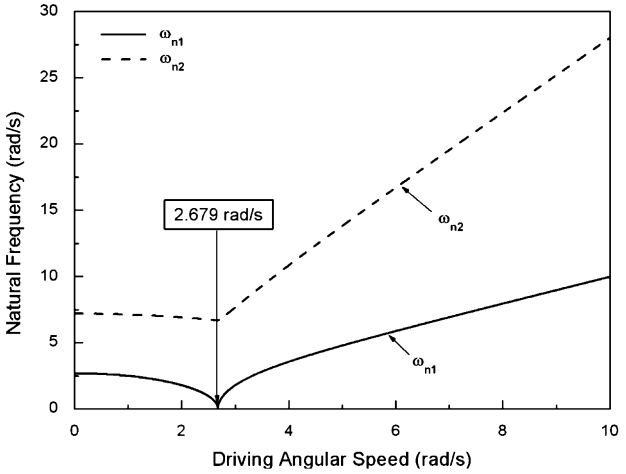

Fig. 3. Variations of the first and the second natural frequencies versus the driving angular speed.

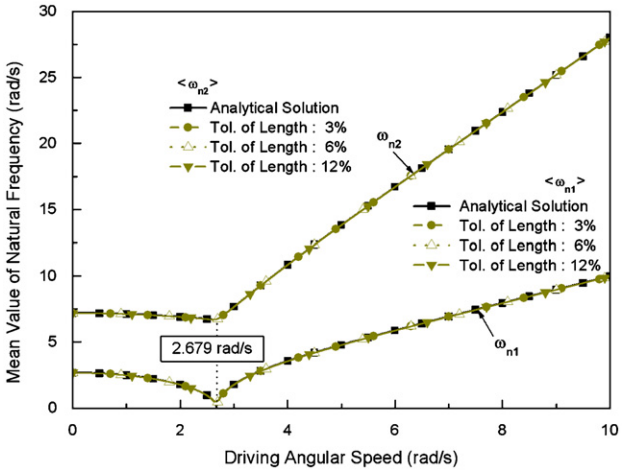

Fig. 4. Comparison of mean values of the natural frequencies (the proposed method versus the Monte-Carlo simulation).

Figs. 5 and 6 show the standard deviations of the first and the second natural frequencies versus the driving angular speed. Three cases of pendulum length tolerances (3.0%, 6.0%, and 12.0%) are employed to obtain the results. As shown, the results obtained by the proposed method are almost identical to the analytical solutions which are obtained with the directly derived equations of motion. As can be expected intuitively, the standard deviations of the natural frequencies increase as the tolerance increases. A few more interesting facts can be noticed from the results too. The standard deviations of the first natural frequency become extremely large around the angular speed 2.679 rad/s while those of the second natural frequency remain relatively small. One can also observe that the standard deviations of the two natural frequencies become sufficiently small as the angular speed keeps increasing.

The results obtained by the proposed method and the Monte-Carlo method, which are compared in Figs. 7 and 8, are generally in good agreement. However, the standard deviations of the first natural frequency obtained by the Monte-Carlo simulation are clearly different from those obtained by the proposed method around the angular speed 2.679 rad/s. For the Monte-Carlo simulation, 3000 samples were employed to obtain the results. Employing more samples would certainly increase the accuracy of the results, but it would also

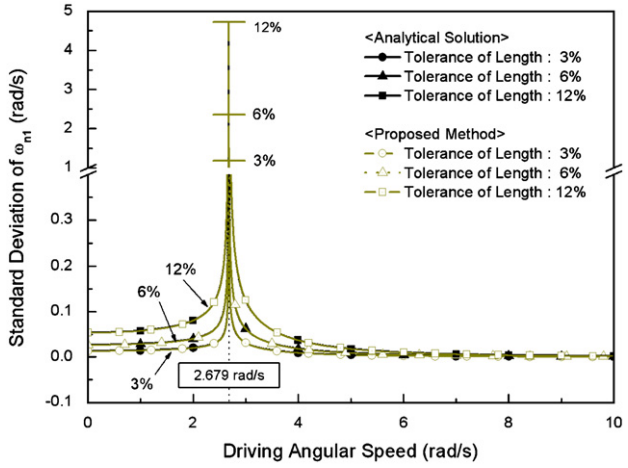

Fig. 5. Comparison of standard deviations of the first natural frequency (the proposed method versus the analytical method).

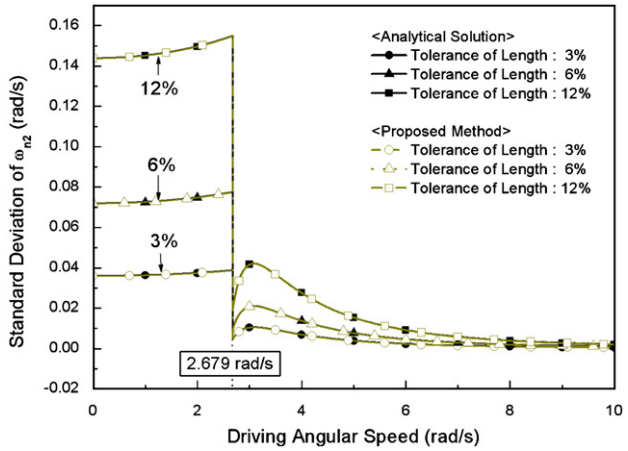

Fig. 6. Comparison of standard deviations of the second natural frequency (the proposed method versus the analytical method).

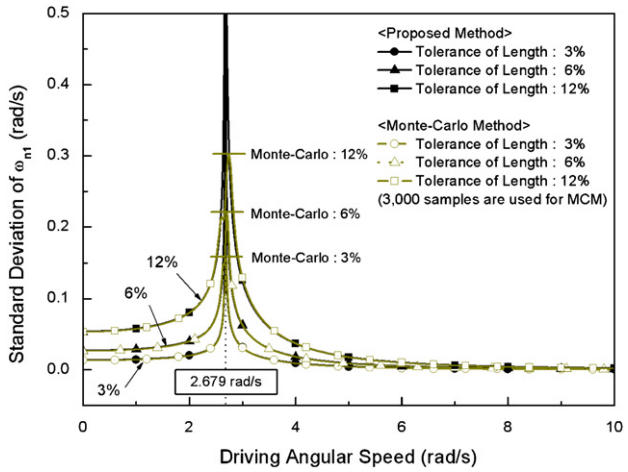

Fig. 7. Comparison of standard deviations of the first natural frequency (the proposed method versus the Monte-Carlo simulation).

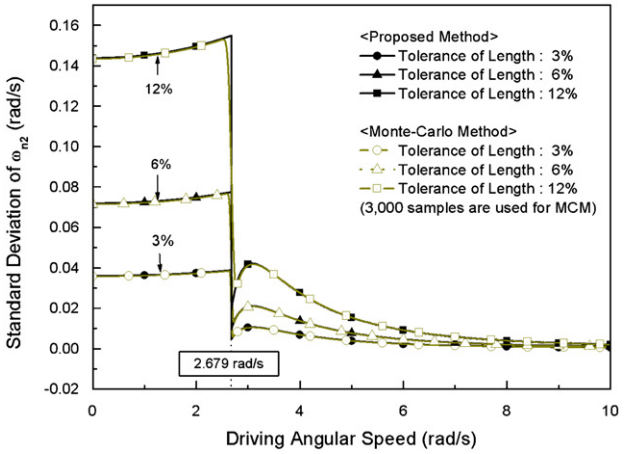

Fig. 8. Comparison of standard deviations of the second natural frequency (the proposed method versus the Monte-Carlo simulation).

Table 1
Comparison of CPU time between the proposed method and the Monte-Carlo simulation (for double pendulum)

Method	CPU time (s)	Ratio
Proposed method	3.297	1
Monte-Carlo method	3286	997

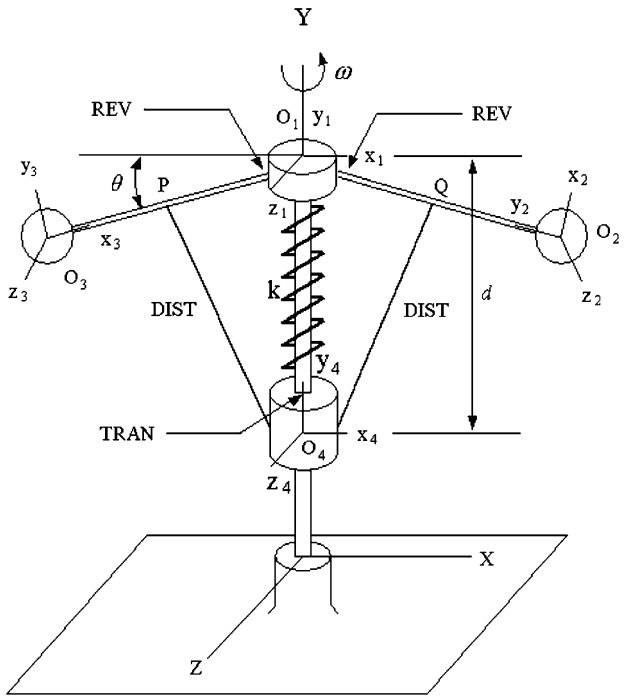

Fig. 9. Configuration of a governor mechanism.

lead to a prohibitively long computation time. Table 1 shows the comparison of CPU time consumed by the proposed method and the Monte-Carlo simulation. As shown in the table, even with the 3000 samples, the Monte-Carlo method consumes much larger computation time. As the number of parts (or degrees of

freedom) of the multi-body system increases, the CPU time increases exponentially. So, employing more than 3000 samples for the Monte-Carlo simulation for practical problems is almost impossible.

Fig. 9 shows a governor mechanism which has two closed kinematic loops. Body 1 of the system is the spindle which is driven by a constant angular speed, bodies 2 and 3 are pendulums which have a sphere mass at each end, and body 4 is the collar. The spindle and the pendulums are connected by revolute joints; the spindle and the collar are connected by a translational joint, a damper and a spring; and the collar and the pendulums are connected by distance joints having fixed distance of 0.1092 m. The damping constant of the damper is 400 N s/m. The stiffness and the free length of the spring are 1000 N/m and 0.15 m, respectively. The inertial properties of the governor mechanism's parts are given in Table 2, and the initial positions of some points in the governor mechanism are given in Table 3.

Fig. 10 shows the mean values of the natural frequency (obtained with the proposed method and the Monte-Carlo simulation) versus the spindle angular speed for three different tolerances of the spring constant.

Table 2
Inertia properties of the parts which constitute the governor mechanism

Body	Mass (kg)	Moment of inertia (kg m^2)		
		I_{xx}	I_{yy}	I_{zz}
Spindle	200.0	25.0	50.0	25.0
Ball 1	1.0	0.1	0.1	0.1
Ball 2	1.0	0.1	0.1	0.1
Collar	1.0	0.15	0.125	0.15

Table 3
Initial positions of some points in the governor mechanism

Point	Initial position (m)
O_1	[0.0, 0.2, 0.0]
O_2	[−0.16, 0.2, 0.0]
O_3	[0.16, 0.2, 0.0]
O_4	[0.0, 0.1256, 0.0]
P	[−0.08, 0.2, 0.0]
Q	[0.08, 0.2, 0.0]

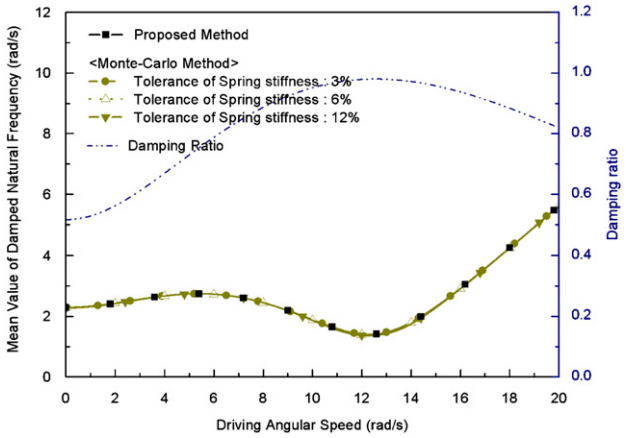

Fig. 10. Mean values of the natural frequency for three tolerances of spring constant (the proposed method versus the Monte-Carlo simulation).

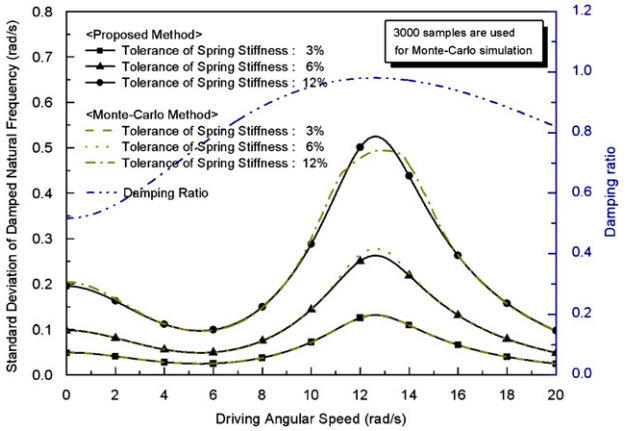

Fig. 11. Standard deviations of the natural frequency for three tolerances of spring constant (the proposed method versus the Monte-Carlo simulation).

Table 4
Comparison of CPU time between the proposed method and the Monte-Carlo simulation (for the governor mechanism)

Method	CPU time (s)	Ratio
Proposed method	2.188	1
Monte-Carlo method	2525	1154

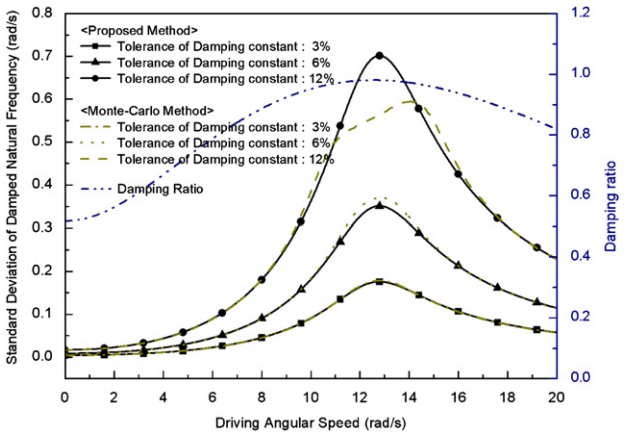

Fig. 12. Standard deviations of the natural frequency for three tolerances of damping constant (the proposed method versus the Monte-Carlo simulation).

As shown, the results obtained with the two methods are in good agreement. The variation of the damping ratio is also shown in the figure. The mean values of the damped natural frequency reach their minimum values when the damping ratio reaches its maximum value (slightly less than 1.0).

Fig. 11 shows the standard deviations of the natural frequency versus the driving angular speed for three different tolerances of spring constant. The results obtained by the proposed method are compared with those by the Monte-Carlo simulation. As shown, the standard deviations are significantly affected by the variation of tolerance. In particular, the standard deviation becomes large around the angular speed where the damped natural frequency reaches its minimum value. This figure also shows that the error of the results obtained by the Monte-Carlo simulation becomes larger at the angular speed, too. Table 4 shows the comparison of CPU time consumed by the proposed method and the Monte-Carlo simulation.

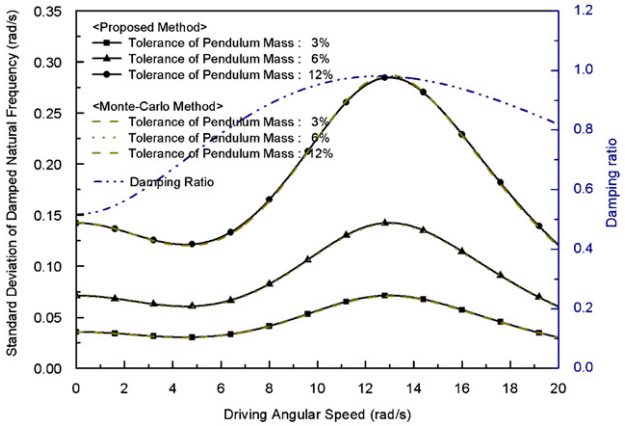

Fig. 13. Standard deviations of the natural frequency for three tolerances of pendulum mass (the proposed method versus the Monte-Carlo simulation).

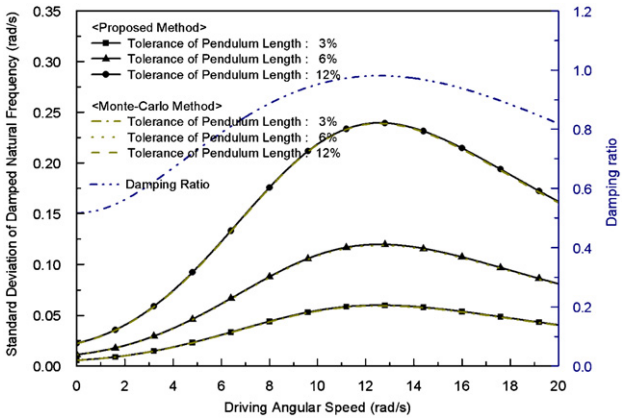

Fig. 14. Standard deviations of the natural frequency for three tolerances of pendulum length (the proposed method versus the Monte-Carlo simulation).

Fig. 12 shows the standard deviations of the natural frequency versus the driving angular speed for three different tolerances of damping constant. The standard deviations become maximized around the angular speed where the damped natural frequency reaches its minimum value. Compared to Fig. 11, discrepancy between the two results obtained by the proposed method and the Monte-Carlo simulation becomes more significant around the angular speed when the tolerance of damping constant is 12%. In general, the tolerance of the damping constant affects the standard deviations of the natural frequency more than that of the spring constant.

Figs. 13 and 14 show the standard deviations of the natural frequency versus the driving angular speed for three different tolerances of pendulum mass and pendulum length. Again, the standard deviations become maximized around the angular speed where the damped natural frequency reaches its minimum value. However, the maximum values of the standard deviations are smaller than the values obtained in the previous figures.

5. Conclusion

A method to analyze the design variable tolerance effect on the natural frequency variance of a constrained multi-body system in dynamic equilibrium is proposed in this study. A sensitivity equation is

derived from an eigenvalue problem for which the mass, damping and stiffness matrices are obtained from a general multi-body formulation. The variance of a natural frequency can be calculated using the sensitivity information which is obtained from the sensitivity equation. A numerical study shows that the proposed method is accurate and much more efficient than the Monte-Carlo simulation. In general the tolerance effect of a design variable on the natural frequency variance varies as the angular speed of the system varies. It is also shown that tolerance effects of some design variables are more significant than those of other design variables. Such information could provide a useful guideline for engineers for the robust design of a mechanical system. The general outline of the procedure is abbreviated in Fig. 15.

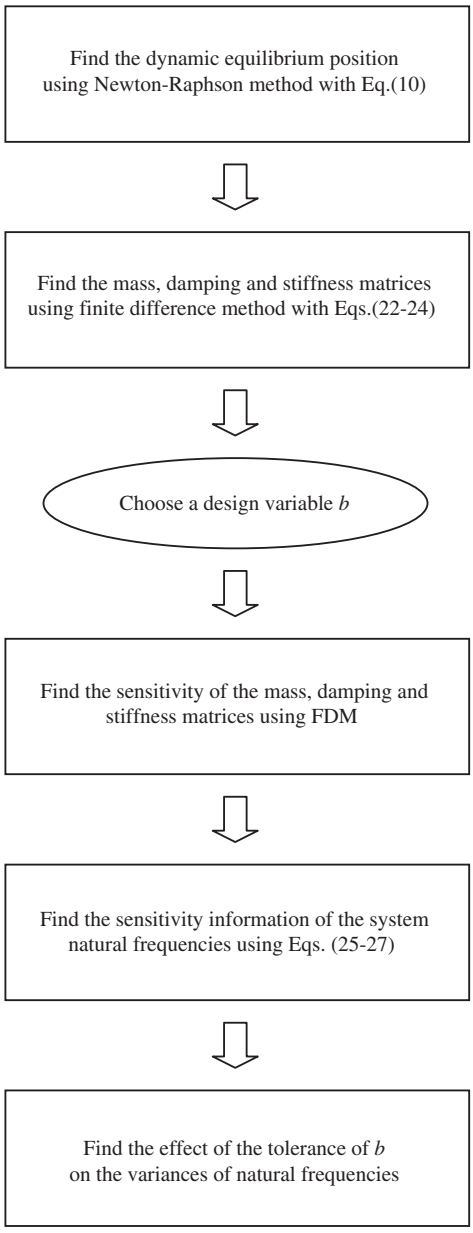

Fig. 15. Procedure to analyze the tolerance effects on the natural frequency variance of a constrained multi-body system in dynamic equilibrium.

References

[1] D.H. Choi, J.H. Park, H.H. Yoo, Steady-state equilibrium analysis of a multibody system driven by constant generalized speeds, *KSME International Journal* 16 (10) (2002) 1239–1245.

[2] S.S. Kim, M. Vanderploeg, A general and efficient method for dynamic analysis of mechanical systems using velocity transformation, *ASME Journal of Mechanism, Transmissions and Automation in Design* 108 (1986) 176–182.

[3] D.S. Bae, E.J. Haug, A recursive formulation for constrained mechanical system dynamics: Part I. Open loop systems, *Mechanics of Structures and Machines* 15 (3) (1987) 359–382.

[4] D.S. Bae, E.J. Haug, A recursive formulation for constrained mechanical system dynamics: Part II. Closed loop systems, *Mechanics of Structures and Machines* 15 (3) (1987) 481–509.

[5] V.N. Sohoni, J. Whitesell, Automatic linearization of constrained dynamical models, *ASME Journal of Mechanisms, Transmissions, and Automation in Design* 108 (1986) 300–304.

[6] D.H. Choi, J.H. Park, H.H. Yoo, Modal analysis of constrained multibody systems undergoing rotational motion, *Journal of Sound and Vibration* 208 (2005) 63–76.

[7] R. Hartenberg, J. Denavit, *Kinematic Synthesis of Linkages*, McGraw-Hill, New York, 1964.

[8] R. Garret, A. Hall, Effects of tolerance and clearance in linkage design, *ASME Journal of Engineering for Industry* 91 (1969) 198–202.

[9] S.J. Lee, Performance Reliability and Tolerance Allocation of Stochastically Defined Mechanical Systems, PhD Dissertation, The Pennsylvania State University, 1989.

[10] S.J. Lee, B.J. Gilmore, The determination of the probabilistic properties of velocities and accelerations in kinematic chains with uncertainty, *ASME Journal of Mechanical Design* 113 (1991) 84–90.

[11] F. Farahanchi, S.W. Shaw, Chaotic and periodic dynamics of a slider-crank mechanism with slider clearance, *Journal of Sound and Vibration* 177 (3) (1994) 307–324.

[12] J. Chunmel, Q. Yang, F. Ling, Z. Ling, The non-linear dynamic behaviour of an elastic linkage mechanism with clearances, *Journal of Sound and Vibration* 249 (2) (2002) 213–226.

[13] E.D. Stoenescu, D.B. Marghitu, Dynamic analysis of a planar rigid-link mechanism with rotating slider joint and clearance, *Journal of Sound and Vibration* 266 (2) (2003) 394–404.

[14] P. Flores, J. Ambrósio, Revolute joints with clearance in multibody systems, *Computers and Structures* 82 (17–19) (2004) 1359–1369.

[15] H. Chun, S.J. Kwon, T. Tak, Multibody approach for tolerance analysis and optimization of mechanical systems, *Journal of Mechanical Science and Technology* 22 (2) (2008) 276–286.

[16] P.E. Nikravesh, *Computer Aided Analysis of Mechanical Systems*, Prentice-Hall, Englewood Cliffs, NJ, 1988.

[17] E.J. Haug, *Computer-Aided Kinematics and Dynamics of Mechanical Systems, vol. I: Basic Method*, Allyn & Bacon, Newton, MA, 1989.

[18] P.E. Nikravesh, *Planar Multibody Dynamics: Formulation, Programming and Applications*, Taylor & Francis, CRC Press, 2007.

[19] J.H. Lim, H.J. Yim, S.H. Lim, T. Park, A study on numerical solution method for efficient dynamic analysis of constrained multibody systems, *Journal of Mechanical Science and Technology* 22 (4) (2008) 714–721.

[20] D.S. Bae, J. Han, H.H. Yoo, Generalized recursive formulation for constrained mechanical systems, *Mechanics of Structures and Machines* 27 (3) (1999) 293–315.

[21] I.W. Lee, G.H. Jung, Natural frequency and mode shape sensitivities of damped systems: Part I, distinct natural frequencies, *Journal of Sound and Vibration* 222 (3) (1999) 399–412.

[22] D.H. Choi, S.J. Lee, H.H. Yoo, Dynamic analysis of multi-body systems considering probabilistic properties, *Journal of Mechanical Science and Technology* 19 (1) (2005) 133–139.

[23] X.Y. Li, S.S. Law, Damage identification of structures including system uncertainties and measurement noise, *AIAA Journal* 46 (1) (2008) 263–276.